JOURNAL OF MATERIALS SCIENCE 25 (1990) 4018–4026

Sintering process of Y_2O_3 and Al_2O_3-doped Si_3N_4

OSAMI ABE
Government Industrial Research Institute, Nagoya 1-1 Hirate-cho, Kita-ku, Nagoya 462, Japan

The sintering process of Y_2O_3- and Al_2O_3-doped Si_3N_4 has been investigated by dilatometry and microstructural observations. The densification progressed through three processes. The bulk density increased to 85% theoretical without the formation of β-Si_3N_4 in the initial process. The densification once terminated after the second process. The α/β transformation of Si_3N_4 and the related formation of prismatic grains reduced the densification rate in the second process, although the grain size and the aspect ratio were very small. The final process was the densification of β-Si_3N_4, where the fibrous grains grew remarkably. The kinetic order for the densification of α-Si_3N_4 indicated a diffusion-rate controlling mechanism with the activation energy of 244 kJ mol^{-1} (<1450° C) and 193 kJ mol^{-1} (>1450° C). The influence of heating rate on the grain growth was characterized by a parameter derived from kinetic parameters. The relationships between grain growth and densification behaviour have also been discussed.

1. Introduction

Liquid-phase sintering process and α/β transformation of silicon nitride have been investigated on the addition of MgO [1–8], Y_2O_3 [5, 8], Y_2O_3–Al_2O_3 [9, 10] and other oxides [11–14]. Most of the kinetic studies were made on the hot-pressing of MgO-doped Si_3N_4, because shrinkage is easily detectable during hot-pressing. There are few studies on the mechanisms and kinetics during pressure-less and gas-pressure sintering and on the relation between densification behaviour and grain growth, which results in the high strength and high fracture toughness of Si_3N_4 ceramics.

The densification process of Y_2O_3-doped Si_3N_4 in an atmosphere of nitrogen gas (1.0 MPa) was investigated previously using a specially assembled dilatometer [15–17]. In the previous study, it was considered that the rate-determining step was the solution of Si_3N_4 into the eutectic melts during the initial sintering. The improved sinterability for recently obtainable powders was characterized by an activation energy lower than the dissociation energy of the Si–N bond. It was indicated that the precise dilatometry was useful for the detailed kinetic studies for the pressure-less sintering. However, the densification processes of Y_2O_3 and Al_2O_3-doped Si_3N_4 have not been investigated in detail, although these additives have been widely used in recent years.

In the present paper, the densification processes of Y_2O_3- and Al_2O_3-doped Si_3N_4 were investigated by dilatometry. The densification mechanism and kinetic parameters are discussed in relation to the growth of fibrous grains.

2. Experimental procedure

2.1. Materials

High-purity α-Si_3N_4 powder (Denka, SNGX) was used as a starting powder. The specific surface area (SSA) and the oxygen content of this powder were 15.3 m^2 g^{-1} and 1.02 wt %, respectively. Amorphous Y_2O_3 (Hokko Chemicals: SSA = 70.9 m^2 g^{-1}) and Al_2O_3 powders (Hokko Chemicals: SSA = 184 m^2 g^{-1}) were used as additives. These powders were vibratory mixed in methanol and dried at 150° C under vacuum after evaporating the methanol at 80° C in flowing nitrogen gas (0.3 kPa). The content of each additive was 3.0 mol % (6.0 mol % in total). Mechanically prepressed green bodies (9 mm × 9 mm × 40 mm) were cold isostatically pressed (CIPed) at 500 MPa for dilatometry. The green density was 1.97 ± 0.02 g cm^{-3}.

2.2. Equipment and procedure

Dilatometry was performed by using a high-temperature dilatometer assembled to study the densification process of non-oxide ceramics. The detail and accuracy of this equipment were discussed previously [16, 18]. The temperature dependence of shrinkage and shrinking rate was measured at a heating rate of 1 to 40 K min^{-1} in a nitrogen atmosphere (pressure 1.0 MPa, gas flow rate 1.0 dm^3 min^{-1}) applying a load of 10 g. For the isothermal dilatometry, the heating rate was 50 K min^{-1} up to the target temperatures. The accuracy of the shrinkage measurement was better than 0.02% for the conditions in the present study [18].

After the dilatometric measurements, the bulk density and porosity were determined by an Archimedean method. Microstructure was observed by scanning electron microscopy (SEM, Jeol, T-330AS). Grain-boundary phases were identified by powder X-ray diffractometry (XRD, Rigaku Denki, RAD-B) with Cu$K\alpha$ radiation at 40 kV and 100 mA. The α-Si_3N_4 content (F_α) was determined from the XRD peak intensities using Equation 1 proposed by Suzuki and Kanno [19]

$$F_\alpha = 1.898 \frac{(I_{\alpha(102)} + I_{\alpha(210)})}{(1.898(I_{\alpha(102)} + I_{\alpha(210)}) + (I_{\beta(101)} + I_{\beta(210)})} \quad (1)$$

0022–2461/90 $03.00 + .12

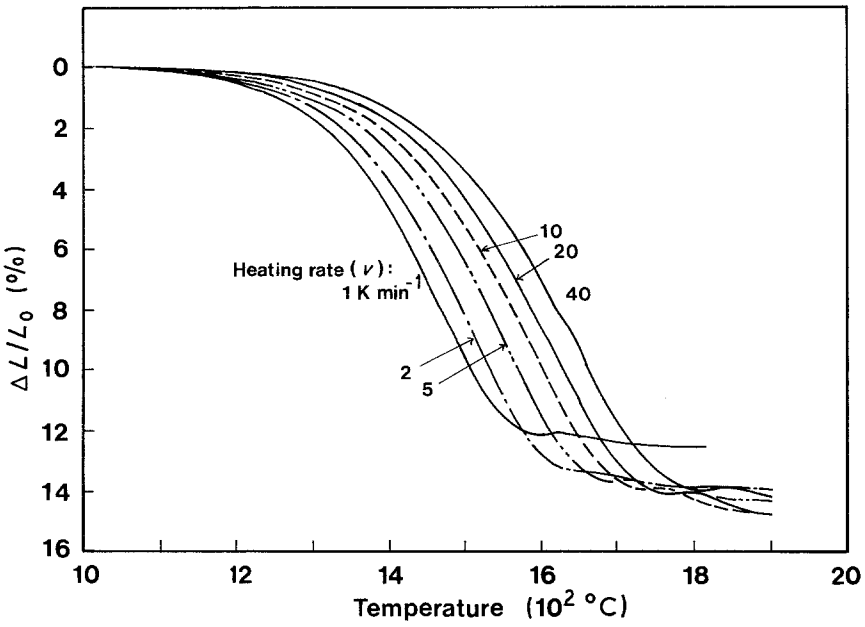

Figure 1 Temperature dependence of shrinkage. Atmosphere N_2 (1.0 MPa); gas flow rate 1.0 dm^3 min^{-1}; load 10 g.

where $I_{\alpha(hkl)}$ and $I_{\beta(hkl)}$ are the integrated peak intensities of (hkl) reflections of α-Si_3N_4 and β-Si_3N_4, respectively.

3. Results

3.1. Temperature dependencies of shrinkage and shrinking rate

Fig. 1 shows the temperature dependence of shrinkage ($\Delta L/L_0$). The shrinking progressed above 1200° C, which was lower than the eutectic temperature in the Y_2O_3–Al_2O_3–SiO_2 triangle (1345° C, [20]). The shrinkage curves shifted toward high temperatures with increasing heating rate (v). The final shrinkage values listed in Table I were higher for the higher heating rate except for the value of 40 K min^{-1} by the termination of shrinkage at lower temperatures. The termination was particularly remarkable at 1 K min^{-1}. The thermal decomposition of the samples was one reason for the termination as described by Mitomo [7], because the samples were heated for long times at low heating rates. However, other factors, such as grain growth and the change of grain shape, could also cause termination in the present case, because there was a remarkable difference in the final shrinkage at 1 and 2 K min^{-1} in spite of the almost same weight loss values as shown in Table I.

The temperature dependence of shrinking rate ($d(\Delta L/L_0)/dt\,v^{-1}$) is shown in Fig. 2. There were no peaks indicating the rearrangement process in spite of liquid-phase sintering. The densification of Y_2O_3- and Al_2O_3-doped Si_3N_4 progressed by at least two processes, I and II, corresponding to Peaks I and II, respectively. Expansions of samples appeared at Min.I after the densification in Process I. The expansion values at Min.I were larger than those estimated from the thermal expansion coefficient of hot-pressed and sintered Si_3N_4 (3.31×10^{-6} K^{-1}/21 to 1315° C, [21]). This indicates an increase in the volume of samples at Min.I.

3.2. Properties and microstructure of sintered materials

Table I shows the properties of materials sintered at 1900° C for 5 min. The bulk density was more than 95% theoretical at a heating rate of 2 to 20 K min^{-1}. The low density obtained at 1 K min^{-1} was caused by the termination of shrinkage at 1650° C. At 40 K min^{-1}, the positive shrinking rate at 1900° C in Fig. 2 suggested a further increase in the bulk density.

The microstructure of materials sintered at 1900° C is shown in Fig. 3. The grain size at 1900° C increased with decreasing heating rate. In the sintered material prepared at 40 K min^{-1} (d), roundish grains remained in addition to fibrous grains with the aspect ratio of 2 to 4. However, the grain size in the transverse direction was not so different from the roundish and fibrous grains at 40 K min^{-1}. At 10 and 5 K min^{-1} (c and b), the sintered bodies consisted of elongated large grains and small grains with small aspect ratios. At 2 K min^{-1} (a), the size of the fibrous grains was two or three times larger than that at 40 K min^{-1}.

Table II shows the properties of samples quenched from Min.I. The α-Si_3N_4 content less than 16% indicated that the α/β transformation of Si_3N_4 had been

TABLE I Influence of heating rate on properties after sintering at 1900° C for 5 min

Heating rate (K min^{-1})	Final shrinkage (%)	Weight loss (%)	α-Si_3N_4 content (%)	Bulk density (g cm^{-3})	Closed porosity (%)	Shrinkage (%) and (temperature, °C) at		
						Peak I	Min.I	Peak II
1.0*	12.56	7.2	tr.	3.04	1.85	8.48(1479)	12.15(1619)	12.18(1643)
2.0	13.98	7.0	tr.	3.11	1.74	9.06(1505)	13.35(1657)	13.47(1684)
5.0	14.29	5.6	0	3.13	1.81	9.20(1545)	13.62(1698)	13.72(1730)
10.0	14.68	4.5	0	3.10	2.29	9.35(1590)	13.83(1747)	14.15(1792)
20.0	14.74	3.9	0	3.08	2.93	9.49(1619)	14.01(1783)	14.19(1825)
40.0	14.11	3.5	0	2.99	3.62	9.24(1648)	13.91(1825)	14.10(1879)

*At 1830° C for 10 sec.

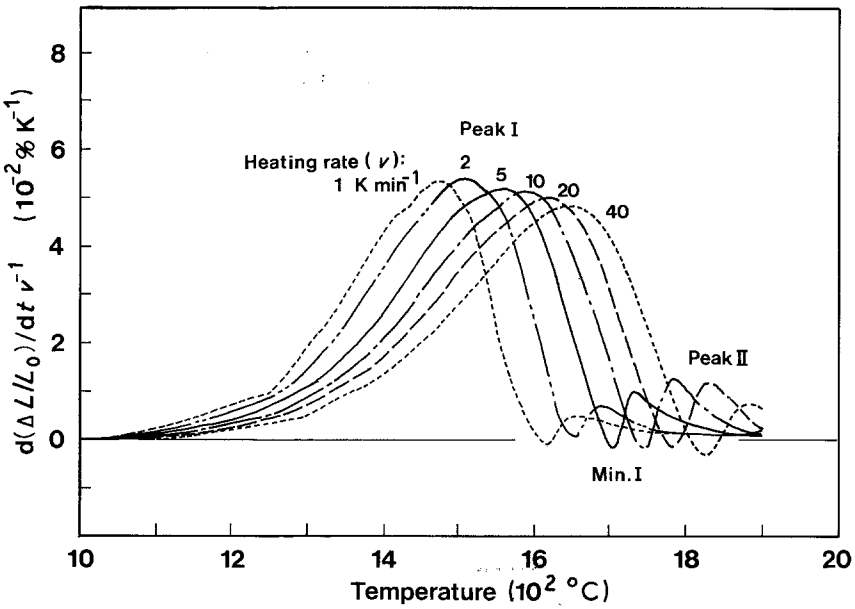

Figure 2 Temperature dependence of shrinking rate. Atmosphere N_2 (1.0 MPa); gas flow rate 1.0 $dm^3\,min^{-1}$; load 10 g.

almost completed at Min.I. At Min.I, the α-Si_3N_4 content was larger at higher heating rates in spite of the higher temperature for Min.I. On the other hand, the α-Si_3N_4 content was more than 90% at Peak I, irrespective of the peak temperatures.

The microstructure at Min.I is shown in Fig. 4. Prismatic grains were observed for both heating rates. At a heating rate of 5 K min^{-1}, the sintered body consisted of larger grains with smaller aspect ratio. On decreasing the heating rate, the grains became elongated with a small grain size. At Peak I, roundish grains were observed at both heating rates, and the grain size was smaller at 2 K min^{-1} than at 5 K min^{-1}. The growth of roundish grains at Peak I suppressed the formation of elongated prismatic grains (fibrous grains) at Min.I.

3.3. Properties of isothermally densified materials

Table III shows the properties of isothermally sintered materials. The densification progressed slowly below 1500° C without α/β transformation of Si_3N_4. At 1500 to 1650° C, the bulk density increased to 2.79 to 2.93 g cm^{-3} accompanying the α/β transformation. However, the rate of the transformation was not so high. After sintering for 2 h, the remaining α-Si_3N_4 was 84% to 25%. Above 1700° C, the densification progressed rapidly with rapid transformation. The

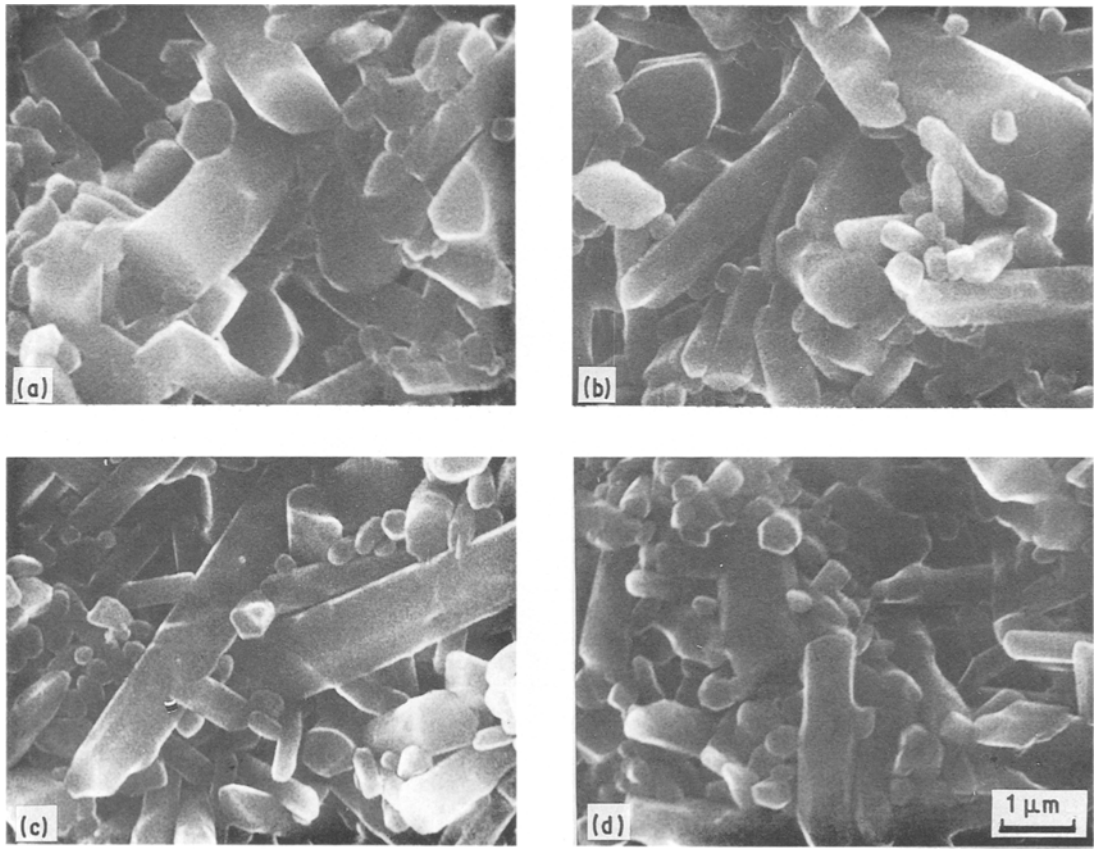

Figure 3 Microstructure of materials sintered at 1900° C for 5 min. Heating rate: (a) 2, (b) 5, (c) 10, (d) 40 K min^{-1}.

TABLE II Properties of quenched samples from temperatures for Min.I

Heating rate ($K\,min^{-1}$)	Temperature (°C)	Weight loss (%)	Bulk density ($g\,cm^{-3}$)	α-Si_3N_4 content (%)	Closed porosity (%)
2	1655	2.9	2.85	5.6	4.88
5	1705	2.5	2.88	12.1	4.79
20	1780	2.2	2.94	16.1	4.37

closed porosity increased at 1550 to 1650° C accompanying the formation of fibrous grains, and then decreased again at 1700 to 1800° C.

The microstructure of the materials is shown in Fig. 5. Few fibrous grains were observed at 1350 to 1550° C after sintering for 2 to 3 h. The fibrous grains with small size and small aspect ratio were observed at 1600° C. At 1650 and 1700° C, the sintered bodies consisted of two kinds of grains; fibrous large grains and roundish small grains. On increasing the temperature up to 1750° C, the grain size and the content of fibrous grains increased. At 1800° C, the grain size decreased again. This decreasing tendency indicates that the densification predominantly progressed rather than the anisotropic grain growth at 1800° C.

No grain-boundary crystalline phases were identified by XRD up to 1650° C at 5 $K\,min^{-1}$. Extremely weak reflections of $10Y_2O_3 \cdot 9SiO_2 \cdot Si_3N_4$, $Y_2O_3 \cdot Si_3N_4$ and $4Y_2O_3 \cdot SiO_2 \cdot Si_3N_4$ were observed above 1650° C. No reflections of grain-boundary phases were detected for quenched unsoaked samples at 1500 and 1600° C. The grain boundary was glassy during isothermal densification.

3.4. Kinetic parameters

The roundish grains observed at 1350 to 1600° C showed that the densification of Y_2O_3- and Al_2O_3-doped Si_3N_4 could be kinetically analysed according to Kingery's model [22, 23].

$$\Delta L/L_0 = kr^{-m}t_c^{-n} \quad (2)$$

where k is the kinetic constant, r the grain size, t_c the corrected soaking time and m, n are constants.

The slow α/β transformation rate below 1650° C indicated that kinetic parameters for densification of α-Si_3N_4 were obtained in the initial stage of sintering. To obtain the kinetic order, the isothermal shrinkage at 1350 to 1700° C was plotted against the corrected soaking time on a log–log scale as shown in Fig. 6. The soaking time was corrected by using approximately linear relations between the shrinking rate and the logarithm of soaking time within 2 min after attaining the target temperatures. The kinetic order obtained from the slope of the linear relations in Fig. 6 was 0.35 to 0.37. The diffusion-rate controlling mechanism was predominant for the initial sintering.

The kinetic constants were obtained from the slopes in Fig. 7. The Arrhenius plot shown in Fig. 8 indicates two linear relations below and above 1450° C. The activation energies for the low (< 1450° C) and high (> 1450° C) temperature ranges were 244.0 and 193.1 $kJ\,mol^{-1}$, respectively.

4. Discussion

4.1. Densification process of Y_2O_3- and Al_2O_3-doped Si_3N_4

The densification process of Y_2O_3- and Al_2O_3-doped Si_3N_4 was roughly classified into Processes I and II from the temperature dependence of the shrinking rate. By referring to the α-Si_3N_4 content at Peak I and Min.I, Process I could be further divided into two sub-processes. That at temperatures up to Peak I (Process Ia) was the densification of α-Si_3N_4 with the growth of roundish grains. The other at temperatures between Peak I and Min.I (Process Ib) was the densification accompanying the α/β transformation of Si_3N_4 and the formation of prismatic grains. The formation of prismatic grains resulted in the decrease of the densification rate in Process Ib. The expansion at Min.I was caused by interlocked structures of prismatic or fibrous grains. The interlocking was suggested by the increase of the closed porosity, although the grain size and the aspect ratio were very small during densification in Process Ib.

In Process II, the densification progressed through the solution–diffusion–reprecipitation of β-Si_3N_4, because the α/β transformation had been almost completed at Min.I. The growth of fibrous grains progressed remarkably during densification in Process II. The decrease of the closed porosity was promoted by the reshaping of β-Si_3N_4 grains in Process II. The increasing gas pressure in the closed pores with increasing temperature may promote the solution of gaseous elements into the grain boundary to increase the shrinking rate.

The anisotropic grain growth in Process II was

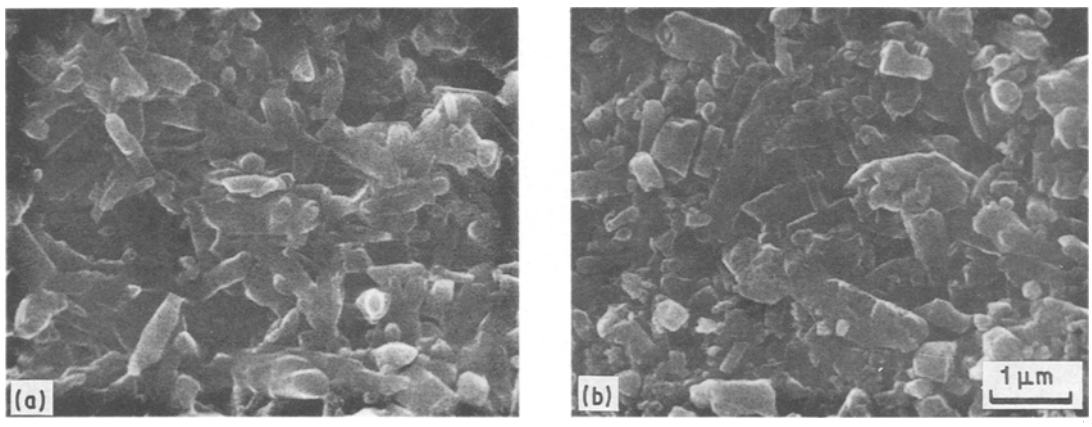

Figure 4 Microstructure of quenched materials from Min.I. Heating rate: (a) 2 $K\,min^{-1}$, 1655° C; (b) 5 $K\,min^{-1}$/1705° C.

TABLE III Properties of isothermally sintered materials

	1350° C (3 h)	1400° C (2 h)	1450° C (2 h)	1500° C (2 h)	1550° C (2 h)	1600° C (2 h)	1650° C (2 h)	1700° C (2 h)	1750° C (2 h)	1800° C (2 h)
Bulk density ($g\,cm^{-3}$)	2.07	2.16	2.30	2.59	2.79	2.87	2.93	3.01	3.09	3.13
Closed porosity (%)	1.77	1.78	1.75	1.83	2.31	4.41	4.59	3.54	2.60	2.18
Weight loss (%)	0.8	1.1	1.4	1.6	2.0	2.3	2.7	3.1	3.6	3.9
α-Si_3N_4 content (%)	96.8	95.2	92.7	92.0	84.0	46.4	25.0	tr.	0	0

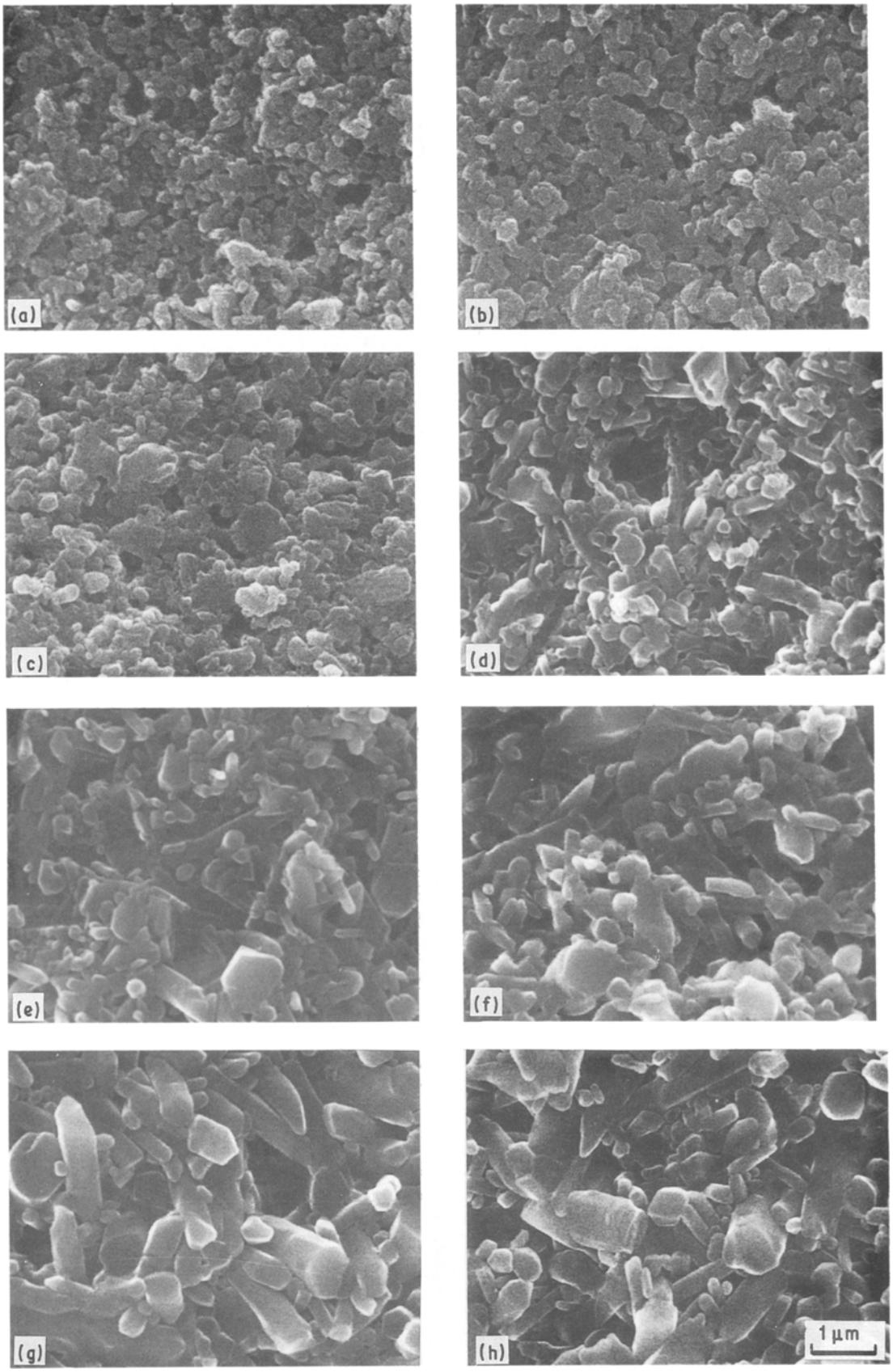

Figure 5 Microstructure of isothermally sintered materials. (a) 1350° C, (b) 1500° C, (c) 1550° C, (d) 1600° C, (e) 1650° C, (f) 1700° C, (g) 1750° C and (h) 1800° C.

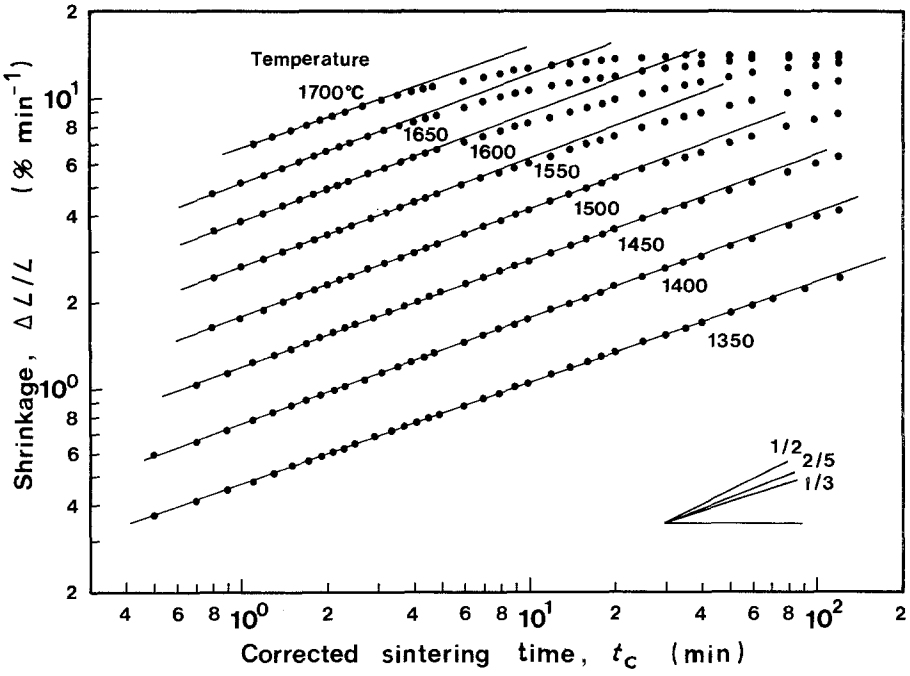

Figure 6 Log–log plots of shrinkage against corrected soaking time.

affected by the density and microstructure at Min.I. The high heating rate increased the shrinkage and the bulk density at Peak I and Min.I as shown in Table I. Thus the contribution of Process I to the growth of roundish grains on the resulting microstructure with small grain size after sintering at 1900° C was increased. At low heating rates, fibrous grains had already been observed at Min.I. These grains grew further during densification in Process II to increase the size of the fibrous grains.

The diffusion-rate controlling densification of α-Si_3N_4 in Process Ia indicated two linear relations in the Arrhenius plot. Bowen *et al.* [1] also reported two linear kinetic relations for the densification of MgO-doped Si_3N_4 below and above 1550° C. They described that the higher activation energy at the low temperature range was caused by the slow diffusion of Si/N atoms through solid grain-boundary phases. In the Y_2O_3–Al_2O_3–SiO_2 phase diagram, the lowest eutectic temperature was 1435° C for SiO_2- and Al_2O_3-rich compositions. However, on the tie line of SiO_2–Y_2O_3–Al_2O_3 [20], the liquidus temperature was about 1450° C. In the present study, the addition of equimolar parts of Y_2O_3 and Al_2O_3 indicated that these additives incompletely converted into the eutectic melt below the liquidus temperature. This suggested that the densification below 1450° C was influenced by the diffusion through a solid grain boundary, as described by Bowen *et al.* [1].

The activation energy below 1450° C (244.0 kJ

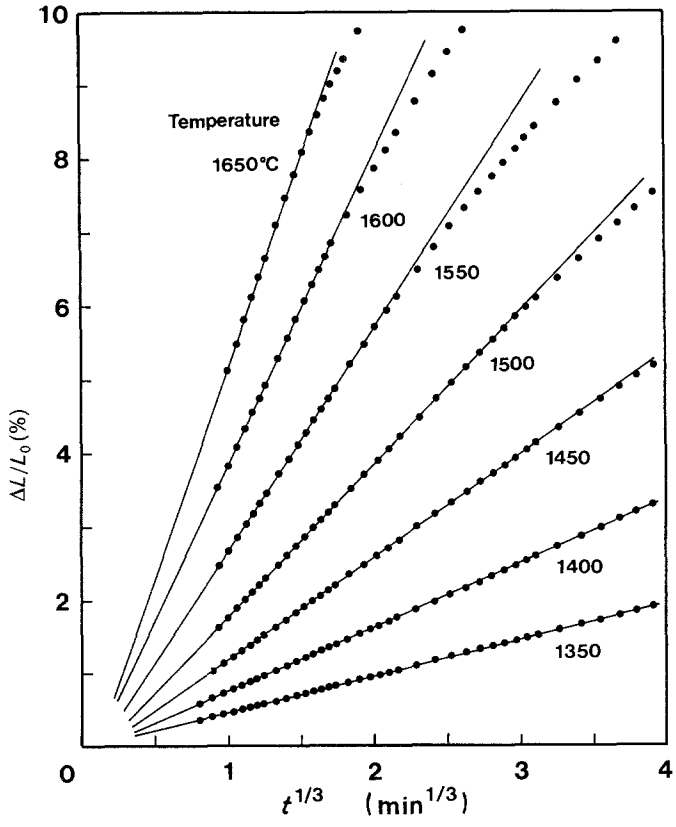

Figure 7 Kinetic plots of shrinkage assuming the diffusion-rate controls sintering. The slopes indicate the kinetic constants.

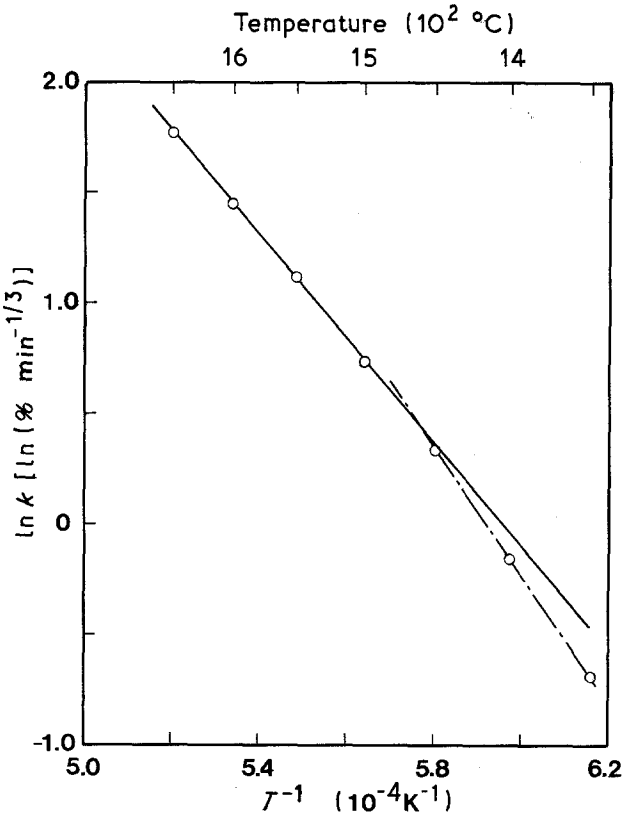

Figure 8 Arrhenius plot for diffusion-rate controlled sintering.

mol^{-1}) was close to that for the diffusion of the nitrogen atom in α-Si_3N_4 (230.12 kJ mol^{-1}) described by Kijima and Shirasaki [24]. The kinetic order of 0.35 to 0.37 was slightly higher than 0.33 for the liquid-phase sintering with diffusion-rate control. These results also suggested the influence of the diffusion of nitrogen atoms through a solid grain boundary. The higher activation energy for the diffusion of nitrogen atoms in other papers [25–27] would be affected by α/β transformation of Si_3N_4, because a higher activation energy (774.0 kJ mol^{-1}) was reported for diffusion in β-Si_3N_4 [24].

Above 1450° C, the densification progressed by the diffusion of Si/N atoms in the liquid phase. The activation energy obtained for the temperature range (193.1 kJ mol^{-1}) was higher than that for the diffusion of nitrogen atoms in SiO_2 glass (109 kJ mol^{-1} [28]). Jack [29] reported that rigidly coordinated nitrogen atoms in the glass network structures increased the viscosity. It was expected that the rigid co-ordination would suppress the migration of nitrogen atoms in the liquid grain-boundary phases to increase the activation energy.

4.2. Influence of heating rate on the grain growth

In the previous papers [15–17], the influence of heating rate on the microstructure was characterized by a parameter (G) indicating the relative grain growth during sintering at individual shrinkages. The parameter was expressed by

$$G = r_2/r_1 = \exp\left[(\Delta E_a - \Delta E)(T_2^{-1} - T_1^{-1})m^{-1}R^{-1}\right] \quad (3)$$

where r_2/r_1 is the relative grain size between the heating rate of v_1 and v_2, ΔE the activation energy obtained by isothermal dilatometry, m a constant, R the gas constant, and T_1 and T_2 the temperatures at v_1 and v_2 for individual shrinkages. The constant (m) was 3/4 for diffusion-rate control. The apparent activation energy (ΔE_a) was obtained from Equation 4 proposed by Ozawa [30] and Doyle [31]

$$\log v = (\text{const.}) - 0.4567\Delta E_a/RT \quad (4)$$

Fig. 9 shows the Ozawa–Doyle plots. The ΔE_a obtained from Equation 4 was 620 to 645 kJ mol^{-1} at shrinkages of 0.5 to 9.0%. The formation of prismatic and/or fibrous grains resulted in the deviation from

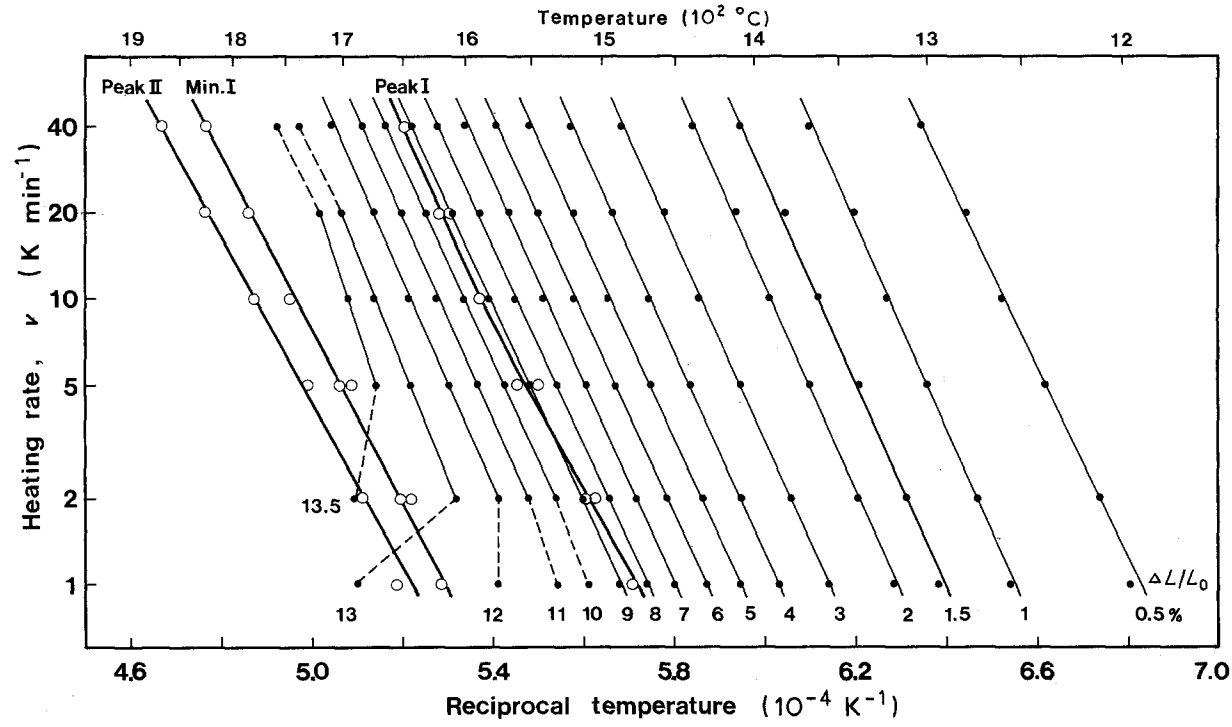

Figure 9 Ozawa–Doyle plots.

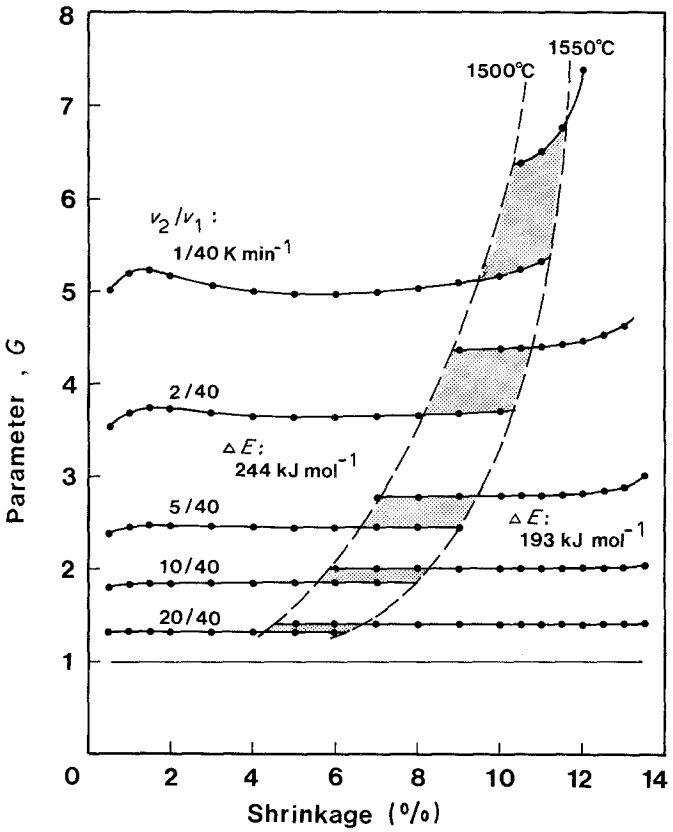

Figure 10 Parameter indicating relative grain growth as a function of shrinkage.

linear relationships in the temperature range between Peak I and Min.I. The temperatures for Peak I also deviated from a linear relation at the low heating rates.

Fig. 10 shows parameter G indicating relative grain growth at 1 to 20 K min^{-1} (v_2) plotted against that at 40 K min^{-1} (v_1) as a function of shrinkage. ΔE values used for the calculation were 244 and 193 kJ mol^{-1} for the range of low and high shrinkages, respectively. For the densification in Process Ib and II, ΔE was assumed to be 193 kJ mol^{-1}, because the rate determination step was considered to be the diffusion through liquid grain-boundary phases. In these processes, the parameter included the influence of the change in grain shape induced by the α/β transformation.

The parameter suggested that the grain size at 2 K min^{-1} was 3.5 to 4.5 times larger than that at 40 K min^{-1}. However, the observed grain size ratio was 2 to 3 as shown in Fig. 3. The disagreement was caused by the influence of the distribution of the size and shape of grains. The thermal decomposition of the samples may also disturb the densification and thus increase parameter G.

The almost constant values of parameter G at shrinkages less than 9.0% (at Peak I) could be replotted linearly against log (v_2/v_1). This indicated that the growth of roundish grains at small shrinkages occurred systematically with increasing heating time. However, above a shrinkage of 9.0%, where the anisotropic grain growth took place with the α/β transformation of Si_3N_4, parameter G increased remarkably at low heating rates. These results suggested the possibility of further optimizing microstructure of Si_3N_4 ceramics by controlling the heating profile during sintering.

References

1. L. J. BOWEN, R. J. WESTON, T. G. CARRUTHERS and R. BROOK, *J. Mater. Sci.* **13** (1978) 341.
2. L. J. BROWN, T. G. CARRUTHERS and R. BROOK, *J. Amer. Ceram. Soc.* **61** (1978) 335.
3. G. R. TERWILLIGER and F. F. LANGE, *J. Mater. Sci.* **10** (1975) 1169.
4. *Idem, J. Amer. Ceram. Soc.* **57** (1974) 90.
5. S. HAMPSHIRE and K. H. JACK, *Proc. Brit. Ceram. Soc.* **31** (1981) 37.
6. T. S. YEN, Z. HANRUI, L. WENLAN, S. SHULIN and F. XIREN, in "Microstructure and Properties of Ceramic Materials", edited by T. S. Yen and J. A. Pask (Science Press, Beijin, 1984) p. 155.
7. M. MITOMO, *J. Mater. Sci.* **11** (1976) 1103.
8. D. R. MESSIRER, F. L. RILEY and R. J. BROOK, *ibid.* **13** (1978) 1199.
9. R. E. LOEHMAN and D. J. ROWCLIFFE, *J. Amer. Ceram. Soc.* **63** (1980) 144.
10. M. MITOMO and K. MIZUNO, *Yogyo-Kyokai-Shi* **94** (1984) 96.
11. H. PICKUP, U. EISELE, E. GILBART and R. J. BROOK, in "Non-oxide Technical and Engineering Ceramics", edited by S. Hampshire (Elsevier, London, 1986) p. 41.
12. V. VANDENEEDE, A. LERICHE, F. CANBIER, H. PICKUP and R. J. BROOK, *ibid.*, p. 53.
13. B. SARUHAN, M. J. POMEROY and S. HAMPSHIRE, *ibid.*, p. 69.
14. G. N. BABINI, A. BELLOSI and P. VINCENZINI, *Ceram. Int.* **6** (1980) 91.
15. O. ABE and S. KANZAKI, in "Ceramic Powder Processing Science", edited by H. Hausner, G. L. Messing and S. Hrano (Deutsche Keramische Gesellschaft, Köln, 1989) p. 931.
16. O. ABE, *J. Mater. Sci.* **25** (1990) 4018.
17. O. ABE and S. KANZAKI, in Proceedings of the 8th Symposium on High-temperature Materials, Aichi (Japan), 1988, p. 27.
18. *Idem, J. Ceram. Soc., Jpn Int. Edn.* **97** (1989) 184.
19. K. SUZUKI and Y. KANNO, *Yogyo-Kyokai-Shi* **92** (1984) 101.
20. G. WÖTTING, B. KANKA and G. ZIEGLER, in "Non-

oxide Technical and Engineering Ceramics", edited by S. Hampshire (Elsevier, London, 1986) p. 83.
21. "Engineering Property Data on Selected Ceramics", Vol. I, "Nitrides" (Materials and Ceramics Information Center, Battele, 1976) p. 5.3.3-2.
22. W. D. KINGERY, *J. Appl. Phys.* **30** (1959) 301.
23. *Idem, ibid.* **30** (1959) 307.
24. K. KIJIMA and S. SHIRASAKI, *J. Chem. Phys.* **65** (1976) 2668.
25. J. MUKERJI and S. K. BISBAS, *J. Amer. Ceram. Soc.* **64** (1981) 549.
26. S. K. BISWAS and M. MUKERJI, *ibid.* **63** (1980) 232.
27. A. ATKINSON, P. J. LEATT and A. J. MOULSON, *Proc. Brit. Ceram. Soc.* **22** (1973) 253.
28. R. H. DOREMUS, in "Modern Aspects of the Vitreous State", Vol. II, edited by D. Mackenzie (Butterworth, London, 1962) p. 16.
29. K. H. JACK, *J. Mater. Sci.* **11** (1976) 1135.
30. T. OZAWA, *Bull. Chem. Soc. Jpn.* **38** (1965) 1881.
31. C. D. DOYLE, *Nature* **207** (1965) 290.

Received 2 May
and accepted 29 September 1989